The topology of the ER-resident phospholipid methyltransferase Opi3 of *Saccharomyces cerevisiae* is consistent with in *trans* catalysis

Received for publication, September 17, 2019, and in revised form, December 16, 2019 Published, Papers in Press, January 13, 2020, DOI 10.1074/jbc.RA119.011102

Grzegorz Pawlik[1], **Mike F. Renne**[2], **Matthijs A. Kol**[3], **and Anton I. P. M. de Kroon**[4]

From the Department of Membrane Biochemistry & Biophysics, Bijvoet Center for Biomolecular Research and Institute of Biomembranes, Utrecht University, 3584 CH Utrecht, The Netherlands

Edited by Dennis R. Voelker

Phospholipid *N*-methyltransferases (PLMTs) synthesize phosphatidylcholine by methylating phosphatidylethanolamine using *S*-adenosylmethionine as a methyl donor. Eukaryotic PLMTs are integral membrane enzymes located in the endoplasmic reticulum (ER). Recently Opi3, a PLMT of the yeast *Saccharomyces cerevisiae* was proposed to perform in *trans* catalysis, *i.e.* while localized in the ER, Opi3 would methylate lipid substrates located in the plasma membrane at membrane contact sites. Here, we tested whether the Opi3 active site is located at the cytosolic side of the ER membrane, which is a prerequisite for in *trans* catalysis. The membrane topology of Opi3 (and its human counterpart, phosphatidylethanolamine *N*-methyltransferase, expressed in yeast) was addressed by topology prediction algorithms and by the substituted cysteine accessibility method. The results of these analyses indicated that Opi3 (as well as phosphatidylethanolamine *N*-methyltransferase) has an N-out C-in topology and contains four transmembrane domains, with the fourth forming a re-entrant loop. On the basis of the sequence conservation between the C-terminal half of Opi3 and isoprenyl cysteine carboxyl methyltransferases with a solved crystal structure, we identified amino acids critical for Opi3 activity by site-directed mutagenesis. Modeling of the structure of the C-terminal part of Opi3 was consistent with the topology obtained by the substituted cysteine accessibility method and revealed that the active site faces the cytosol. In conclusion, the location of the Opi3 active site identified here is consistent with the proposed mechanism of in *trans* catalysis, as well as with conventional catalysis in *cis*.

In yeast, Cho2 and Opi3 serve as phospholipid *N*-methyltransferases (PLMTs)[5] converting phosphatidylethanolamine (PE) into phosphatidylcholine (PC) using *S*-adenosylmethionine (SAM) as methyl donor (EC 2.1.1.17). Cho2 catalyzes the first methylation yielding phosphatidylmonomethylethanolamine (PMME), whereas Opi3 catalyzes the two subsequent methylations yielding phosphatidyldimethylethanolamine (PDME) and PC, respectively (1, 2). Opi3 also methylates PE at a low rate (3). In mammals a single PE methyltransferase (PEMT) homologous to Opi3 (4) catalyzes all three steps (5). PEMT is primarily active in the liver where it plays an important role in the synthesis of lipoproteins (6). Plants harbor a PLMT that converts PMME via PDME to PC (7).

The CDP-choline (Kennedy) pathway is the other main source of PC in eukaryotes. In mammals and fungi, the CDP-choline pathway depends on the supply of choline for net synthesis (8), whereas plants contain methyltransferases converting phosphoethanolamine to phosphocholine that serves as substrate (9). By converting SAM into *S*-adenosylhomocysteine (SAH), the PE methylation pathway impacts metabolism of sulfur-containing amino acids (10), and its inactivation was recently shown to lead to accumulation of SAM and hypermethylation of histones and the major phosphatase PP2A in yeast (11).

Two main types of PLMT have been described to date. Several bacterial species harbor a soluble, cytosolic PLMT that synthesizes PC by transiently associating with membranes dependent on the anionic/zwitterionic phospholipid ratio (12). Eukaryotic PLMTs are integral membrane proteins located in the endoplasmic reticulum (ER) (7, 13, 14), from which the synthesized PC can be transported to other cellular compartments via various mechanisms (15).

Yeast Opi3 has recently been proposed to be capable of in *trans* catalysis at membrane contact sites, where membranes stay in very close apposition within a distance of 10–30 nm (16). In *trans* catalysis entails the conversion of lipid substrate in one membrane by an enzyme located in a juxtaposed membrane and has been put forward as a mechanism of intermembrane regulation of lipid composition that avoids the energetically

This work was supported by the Focus en Massa Program Membrane proteins of Utrecht University. The authors declare that they have no conflicts of interest with the contents of this article.

This article contains Table S1 and Fig. S1.

[1] Present address: Liposoma B.V., Science Park 408, 1098 XH Amsterdam, The Netherlands.

[2] Present address: Sir William Dunn School of Pathology, University of Oxford, Oxford OX1 3RE, United Kingdom.

[3] Present address: Molecular Cell Biology Division, Dept. of Biology/Chemistry, University of Osnabrück, 49076 Osnabrück, Germany.

[4] To whom correspondence should be addressed: Dept. of Membrane Biochemistry & Biophysics, Utrecht University, Padualaan 8, 3584 CH Utrecht, The Netherlands. E-mail: a.i.p.m.dekroon@uu.nl.

[5] The abbreviations used are: PLMT, phospholipid *N*-methyltransferase; PC, phosphatidylcholine; SAM, *S*-adenosylmethionine; ER, endoplasmic reticulum; PEMT, phosphatidylethanolamine *N*-methyltransferase; SCAM, substituted cysteine accessibility method; ICMT, isoprenyl cysteine carboxyl methyltransferase; PE, phosphatidylethanolamine; PMME, phosphatidylmonomethylethanolamine; PDME, phosphatidyldimethylethanolamine; SAH, *S*-adenosylhomocysteine; DTR, dual topology reporter; TM, transmembrane domain; aa, amino acid(s); Endo H, endoglycosidase H; Ubi, ubiquitin; *M.a.*, *M. acetivorans*; *T.c.*, *T. castaneum*; SD, synthetic defined; LUV, large unilamellar vesicle; EMCS, 6-maleimido-caproic acid sulfo-*n*-succinimidyl ester.

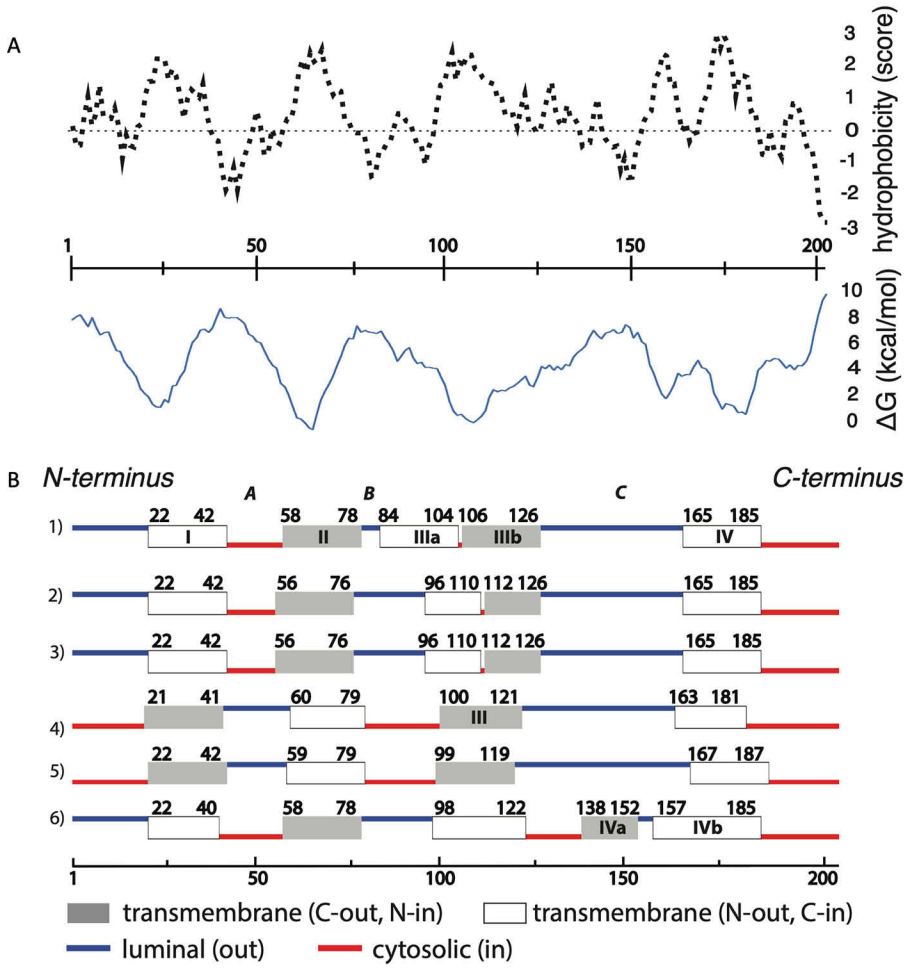

Figure 1. *In silico* predictions of the membrane topology of Opi3. *A*, hydrophobicity plot (*dotted line*) of the Opi3 amino acid sequence generated by ExPASy ProtScale (38) according to Kyte and Doolittle (39), and ΔG_{app} values (*blue line*) for membrane insertion generated by TOPCONS. *B*, Opi3 topology predictions generated by algorithms: TOPCONS (*topology 1*), OCTOPUS (*topology 2*), SPOCTOPUS (*topology 3*), Philius (*topology 4*), SCAMPI (*topology 5*), and PolyPhobius (*topology 6*) using the TOPCONS server. The *numbers* indicate amino acid positions in the Opi3 sequence. Potential transmembrane segments and loops are indicated by *Roman numbers* and *capital letters*, respectively. *Blue* and *red lines* indicate luminal and cytosolic localization of loops, respectively.

expensive efflux of lipids from a donor membrane and transport to the destination membrane (17).

Several lines of evidence support in *trans* catalysis by Opi3. Opi3 in isolated ER membranes (microsomes) from a strain lacking Cho2 (*cho2*Δ) was shown to methylate PMME accumulated in microsomes isolated from an *opi3*Δ mutant (18). Plasma membrane–ER contact sites were shown to be required for PC synthesis *in vivo* by Opi3 using yeast mutant strains with reduced cortical ER (19, 20). In *trans* catalysis by Opi3 is further supported by the ability of microsomal Opi3 to convert PMME in liposomes *in vitro* (20) and more recently by the demonstration that cell-free synthesized Opi3 in nanodisc membranes converts PMME supplied in enzyme-free nanodiscs (21).

A prerequisite for in *trans* catalysis by Opi3 is a cytosolic localization of its active site. So far, attempts to obtain crystal structures of phospholipid methyltransferases have not been successful (22). Shields *et al.* (13, 23) investigated the membrane topology and the localization of the active site of human PEMT, and obtained results consistent with a cytosolic localization of both N and C terminus, as well as the active site.

Here the membrane topology of Opi3 is analyzed using a dual topology reporter (DTR) and by the substituted cysteine accessibility method (SCAM). These methods have recently been applied to analyze the membrane topology of a number of yeast lipid biosynthetic enzymes residing in the ER membrane including PI synthase and several acyltransferases (24–26). The results show that Opi3 contains four transmembrane domains (TMs), with the fourth TM forming a re-entrant loop, and has an N-out C-in topology. Because the membrane topology obtained for Opi3 differs from the topology previously proposed for human PEMT (13), PEMT was expressed in yeast and analyzed by SCAM. The topology obtained for human PEMT was similar to that of Opi3. Based on a comparison with membrane methyltransferases of known structure (27, 28), potential SAM-binding residues in Opi3 were predicted and tested. The active site of Opi3 was found to face the cytosol, consistent with in *trans* catalysis by Opi3.

Results

Membrane topology of Opi3

Opi3 is a 206-aa membrane protein containing four hydrophobic regions according to the hydropathy plot and in agreement with the ΔG_{app} values for membrane insertion (Fig. 1*A*).

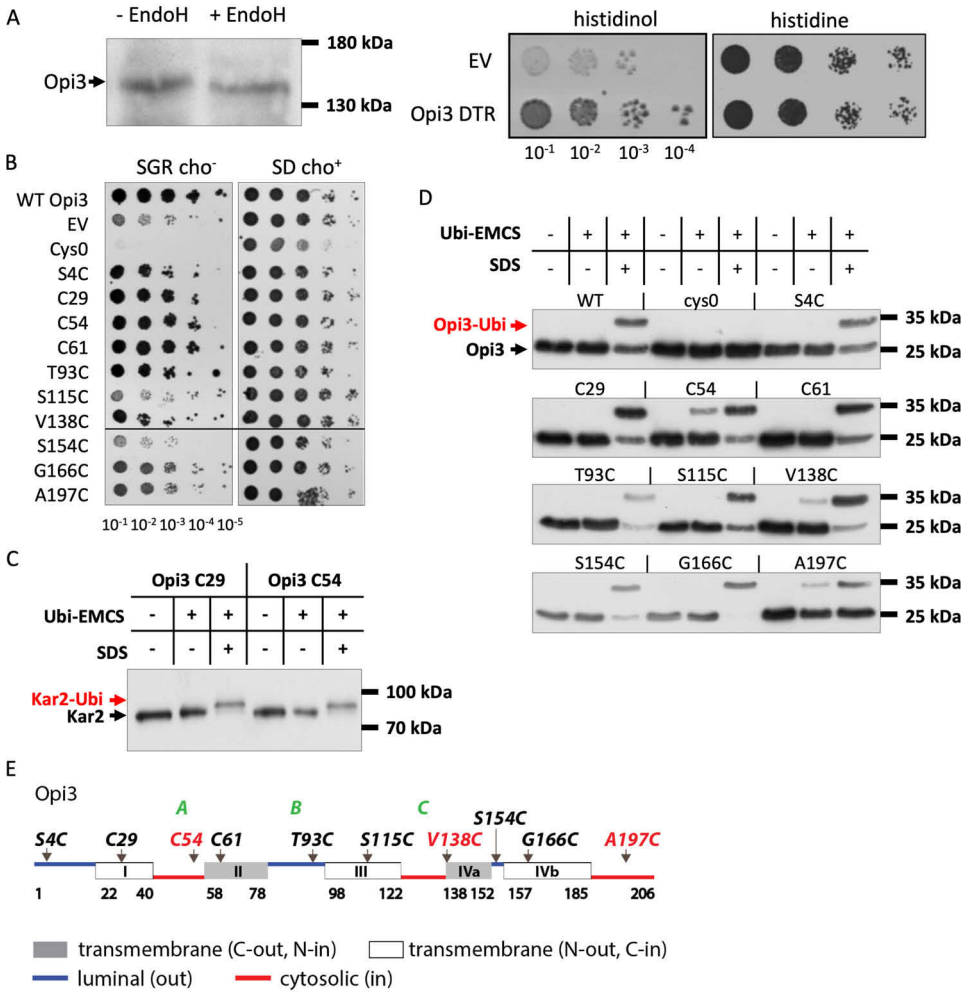

Figure 2. Membrane topology of Opi3. *A*, localization of the C terminus of Opi3 using DTR. Lysates of cells expressing Opi3-DTR were analyzed by Western blotting using anti-HA antibody before and after Endo H treatment (*left panel*). Serial dilution experiment testing the ability of STY50 cells expressing Opi3-DTR *versus* the empty vector control (*EV*) to grow on histidinol and histidine (*right panels*). *B*, complementation test of Opi3 single cysteine mutants. Cells from a *cho2opi3* strain transformed with the pYES2.1 TOPO vector encoding V5-His_6-tagged WT or mutant Opi3 as indicated were serially diluted on synthetic media lacking choline and containing galactose and raffinose (SGR cho^-) to induce expression from the *GAL1* promoter or containing 1 mM choline and glucose (SD cho^+) as a positive control and incubated for 3 days at 30 °C. *EV* denotes the empty vector control. The cells expressing active Opi3 grow in medium containing galactose and lacking choline. *C*, the single cysteine in Kar2 is not accessible to Ubi–EMCS under SCAM conditions in the absence of detergent. Preparations of microsomes from two Opi3 single cysteine mutants were incubated with Ubi–EMCS in the presence and absence of 1% SDS. Ubiquitination was analyzed by Western blotting using anti-Kar2p. *D*, cysteine accessibility in Opi3 in the absence and presence of SDS was probed with Ubi–EMCS using microsomes from *cho2opi3* cells expressing WT, cysteine-free (*cys0*), and single-cysteine Opi3-V5-His_6 constructs as indicated. Ubiquitination was analyzed by Western blotting using antibodies against the C-terminal V5 tag. *E*, SCAM results of Opi3 superimposed on the PolyPhobius topology prediction (*topology 6* in Fig. 1*B*). Accessible (cytosolic) and inaccessible cysteines are indicated in *red* and *black*, respectively, and soluble domains are in *green*. The results are representative of two independent experiments.

TOPCONS algorithms suggest the presence of four or five membrane-spanning domains and a cytosolic localization of the C terminus, whereas the predicted localization of the N terminus varies (Fig. 1*B*). Three types of structure prediction emerge: (i) N-out, C-in following the positive-inside rule (the charge distribution in Opi3 and net charge calculations for the soluble domains predicted by PolyPhobius are shown in Fig. S1*A*), localizing positively charged domain A and the C terminus cytosolically, whereas the other soluble domains localize to the ER lumen, generating a re-entrant loop in TM III (*topologies 1–3* in Fig. 1*B*); (ii) N-in, C-in without any re-entrant loops (*topologies 4* and *5* in Fig. 1*B*); and (iii) N-out, C-in topology with a re-entrant loop in TM IV that corresponds to aa stretch 138–185 (*topology 6* in Fig. 1*B*). Fig. S1*B* shows the apparent free energies for membrane insertion calculated for the TM domains predicted by the algorithms.

The predicted cytosolic localization of the C terminus was tested by attaching the *SUC2–HIS4C* DTR (29) to the C terminus of Opi3. If the C-terminal DTR localizes to the cytoplasm, the His4C fragment allows histidine auxotrophic cells to grow on histidinol, whereas DTR localization in the ER lumen results in a protein size shift upon Endo H treatment caused by *N*-glycosylation of the Suc2 fragment. Fig. 2*A* shows that the Opi3–DTR fusion protein is not Endo H–sensitive and allows growth on histidinol, demonstrating that the C terminus localizes to the cytosol.

To address the full topology of Opi3, SCAM was applied to microsomes (ER-derived vesicles), using ubiquitin–6-maleimido-caproic acid sulfo-*n*-succinimidyl ester (Ubi–EMCS) as membrane-impermeant cysteine-reactive probe that increases protein mass by 9 kDa for each cysteine labeled (24, 25). Because microsomes have a right-side-out membrane orienta-

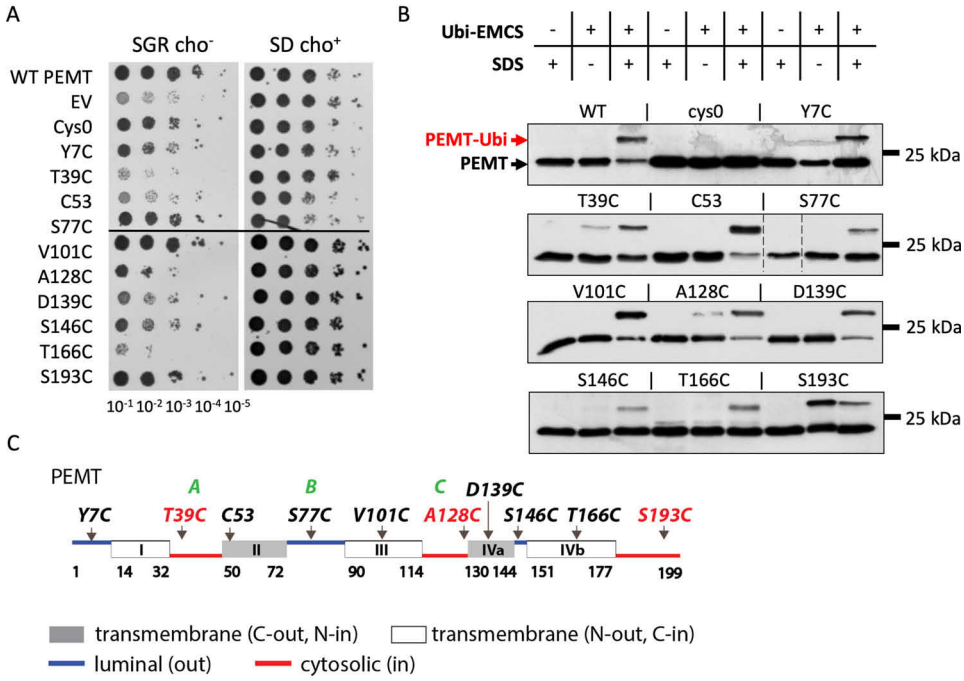

Figure 3. Membrane topology of PEMT. *A*, complementation test of PEMT single-cysteine mutants. The cells from a *cho2opi3* strain transformed with the pYES2.1 TOPO vector encoding V5-His_6-tagged WT or mutant PEMT as indicated were serially diluted on choline-free SGR medium to induce expression from the *GAL1* promoter and on SD medium supplemented with 1 mM choline (positive control) and incubated for 3 days at 30 °C. *EV* denotes the empty vector control. *B*, cysteine accessibility in PEMT in the absence and presence of SDS was probed with Ubi–EMCS using microsomes from *cho2opi3* cells expressing WT, cysteine-free (*cys0*), and the single cysteine PEMT-V5-His_6 constructs as indicated. Ubiquitination was analyzed by Western blotting using antibodies against the C-terminal V5 tag. The *dashed lines* in the *second panel* serve to indicate that the S77C construct was analyzed on a separate gel and that the scan of its blot was spliced to correct an error that occurred during loading of the gel. *C*, SCAM results of PEMT superimposed on the PolyPhobius topology prediction (Fig. S1 and *topology 6* in Fig. 1*B*). Accessible (cytosolic) and inaccessible cysteines are indicated in *red* and *black*, respectively, and soluble domains are in *green*. The results are representative of two independent experiments.

tion, the probe reacts only with cysteines in cytosolic domains. Based on the topology predictions (Fig. 1*B*), a set of single cysteine Opi3 constructs was generated with the cysteine localized in each of the putative transmembrane and soluble domains and equipped with a C-terminal V5-His_6 tag. Single cysteine mutants were obtained by site-directed mutagenesis, replacing three of the four native cysteines (Cys-29, Cys-54, Cys-61, and Cys-89) by serine residues, or by substituting single amino acids by cysteine in a cysteine-free Opi3 background. Subsequently, the constructs were expressed in a *cho2opi3* double deletion mutant. The ability of the plasmid-borne *OPI3* alleles to complement the choline auxotrophy of the *cho2opi3* double deletion mutant was used to test the activity of the single cysteine Opi3 constructs. Upon induction from the *GAL1* promoter, almost all alleles supported growth of the *cho2opi3* strain in choline-free medium, except for S115C, S154C, and the cysteine-free construct (Fig. 2*B*).

Impermeability of the microsomes to Ubi–EMCS under the reaction conditions used was verified by analysis of the soluble luminal protein Kar2 that contains a single cysteine. Only in the presence of detergent was the cysteine modification observed (Fig. 2*C*) in agreement with previous reports (24, 25). Fig. 2*D* shows the results of the cysteine scanning of Opi3. Cys-54 (loop A), V138C (loop C), and Ala-197 (C-terminal part of Opi3) were accessible to reaction with Ubi–EMCS in the absence of detergent, indicating a cytosolic localization. In contrast, S4C (N-terminal part), T93C (putative loop B), and Cys-29, Cys-61, and G166C (in predicted transmembrane domains) (Fig. 1) only reacted with Ubi–EMCS in the presence of detergent. S115C and S154C displayed similar behavior, but these results should be interpreted with caution, because both constructs were not functional (Fig. 2*B*). As expected, all Opi3 variants were modified by Ubi–EMCS in the presence of SDS, except for the cysteine-free construct. The N-out (luminal), C-in (cytosolic) topology is indicative for an odd number of transmembrane segments. The localization of loop C in the cytosol indicates that putative transmembrane segment IV forms a re-entrant loop or is divided into two small transmembrane domains, as predicted by the PolyPhobius algorithm (Fig. 2*E*, compare with *topology 6* in Fig. 1*B*).

Membrane topology of human PEMT

The N-out, C-in Opi3 topology deduced from the SCAM data is at odds with the N-in, C-in topology reported previously for human PEMT (13). PEMT and Opi3 show a high level of sequence conservation (56% sequence similarity and 41% identity according to the EMBOSS Needle server (30)) and corresponding predicted membrane topologies (Fig. S1*A*). Therefore, we decided to extend the SCAM analysis to human PEMT heterologously expressed in yeast. The ability of PEMT expressed from the *GAL1* promoter to suppress the choline auxotrophy of *cho2opi3* yeast cultured on choline-free medium containing galactose (SGR cho^-; Fig. 3*A*) demonstrates that the enzyme adopts a functional conformation and thus can be used for SCAM. SCAM analysis revealed that mutants T39C (loop A), A128C (loop C), and S193C (C terminus) reacted with Ubi–

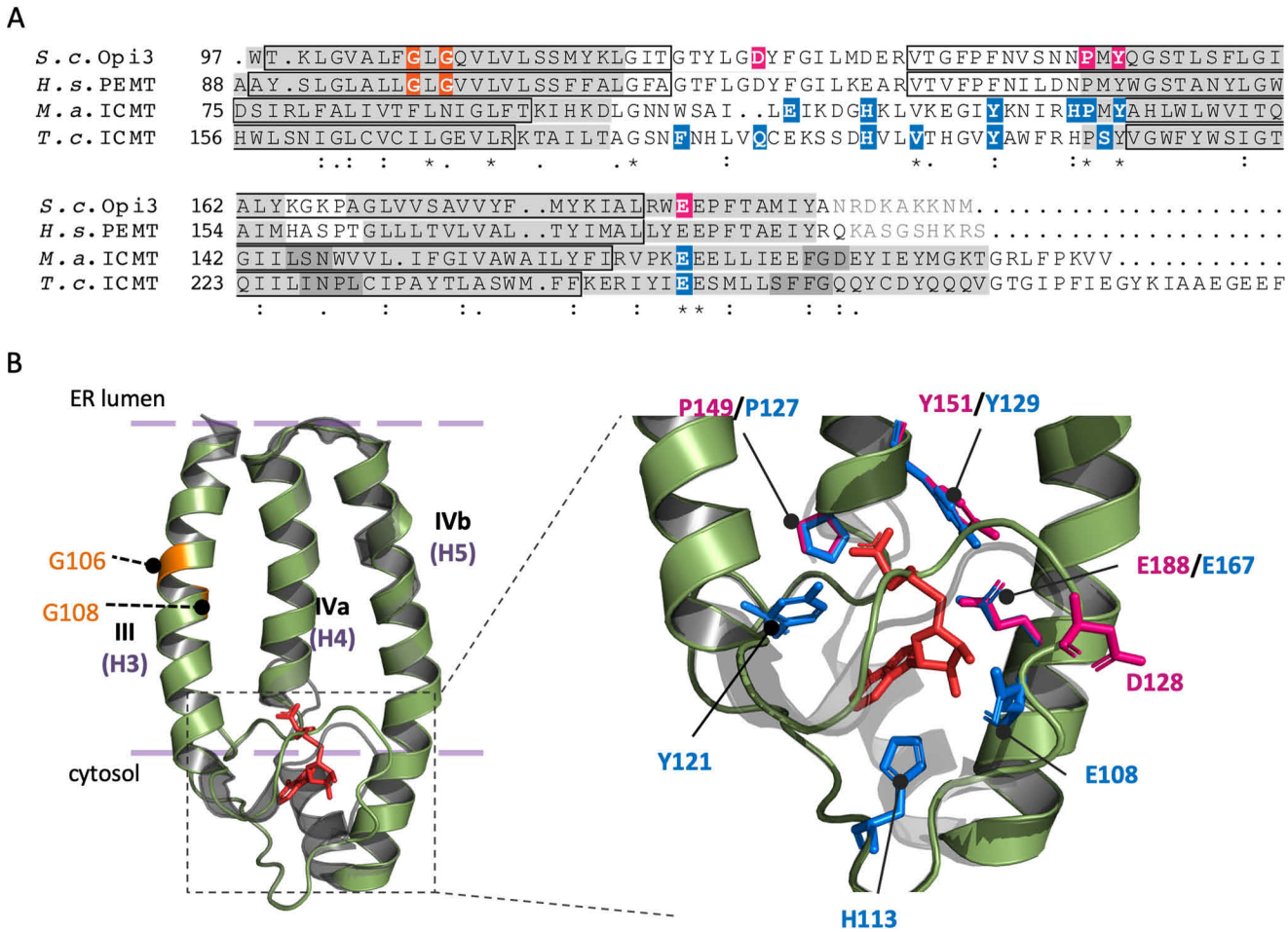

Figure 4. Active site of Opi3. *A*, alignment of the C-terminal amino acid sequences of *S. cerevisiae* Opi3 (*S.c. Opi3*), *Homo sapiens* PEMT (*H.s. PEMT*) *M. acetivorans* ICMT (*M.a. ICTM*), and *T. castaneum* ICMT (*T.c. ICMT*) generated using the UniPRot ALIGN server. *Asterisks*, *colons*, and *dots* indicate sequence identity in descending order. *Black boxes* indicate the positions of TM domains predicted by PolyPhobius (TOPCONS), *light gray highlighting* shows α-helices in the crystal structures of *M.a.* ICMT and *T.c.* ICMT and predicted α-helices (SWISS-MODEL) of *S.c.* Opi3 and *H.s.* PEMT. *Dark gray highlighting* indicates the positions of turns in α-helices; amino acids shown as *light gray letters* were not involved in structure prediction. Amino acids highlighted in *blue* form hydrogen bonds with SAH in the ICMT crystal structures. Amino acids highlighted in *magenta* are proposed to be involved in hydrogen bonding with SAH/SAM in Opi3 and have been mutated to alanines. Glycines previously proposed to interact with SAM in PEMT and the corresponding glycines in Opi3 are highlighted in *orange*. *B*, superposition of the model of the C-terminal part of Opi3 in *green* on the structure of the SAM binding site of *M. acetivorans* ICMT (4a2n) shown in *gray* (*left panel*). The structure of the C-terminal part of Opi3 was modeled using SWISS-MODEL homology modeling software using *M.a.* ICMT structure (4a2n) as a template. *H3*, *H4*, and *H5* are TM domains in *M.a.* ICMT corresponding to Opi3 helices III, IVa, and IVb, respectively. The *right panel* zooms in on the SAM/SAH–binding site with the amino acids forming H-bonds with SAH in *M.a.* ICMT highlighted in *blue*. The amino acids in *magenta* are residues in Opi3 predicted to be involved in binding SAM/SAH. SAH is shown in *red sticks*. *Dashed purple lines* show the approximate localization of the boundaries of the membrane. See text for details.

EMCS reflecting a cytosolic localization, whereas Y7C (N terminus), S77C (loop B), and S146C (loop C) together with Cys-53, V101C, D139C, and T166C did not, indicating a luminal or transmembrane localization (Fig. 3*B*). The results obtained for mutants T39C, Cys-53, and T166C should be interpreted with caution because the growth of strains expressing these alleles is similar to the strain harboring the empty vector control (Fig. 3*A*). The cysteine accessibility scanning of the PEMT and Opi3 constructs yielded consistent results (Figs. 2*E* and 3*C*), indicating that both enzymes share a membrane topology consistent with that predicted by PolyPhobius (Fig. 1*B* and Fig. S1*A*).

Localization of the active site of Opi3

To identify amino acids involved in the catalytic cycle of Opi3, the amino acid sequence of Opi3 was screened for conserved motifs using HHpred software. Three significant hits were found: a putative isoprenyl cysteine carboxyl methyltransferase from *Metanosarcina acetivorans* (*M.a.* ICMT, 4a2n, *E* value 4.5*E*-21) (27), an isoprenylcysteine carboxyl methyltransferase from *Tribolium castaneum* (*T.c.* ICMT, 5v7p, *E* value 3.5*E*-20) (28), and Δ^{14}-sterol reductase from *Methylomicrobium alcaliphilum* (4QUV, 2.7E-15) (31). Here we focus on the similarity between Opi3 (and PEMT) and the two ICMTs because they also use SAM as methyl donor. A relatively high level of similarity is observed in the C-terminal region (aa 98–206 in Opi3), as shown in the alignment with the corresponding sequences of human PEMT, *M.a.* ICMT, and *T.c.* ICMT (Fig. 4*A*). We generated a model of the structure of the C-terminal part of Opi3 (aa 98–206) based on the crystal structure of *M.a.* ICMT (aa 75–194) using the SWISS-MODEL homology modeling server. The amino acids forming hydrogen bonds with SAH the product of SAM demethylation) in *M.a.*

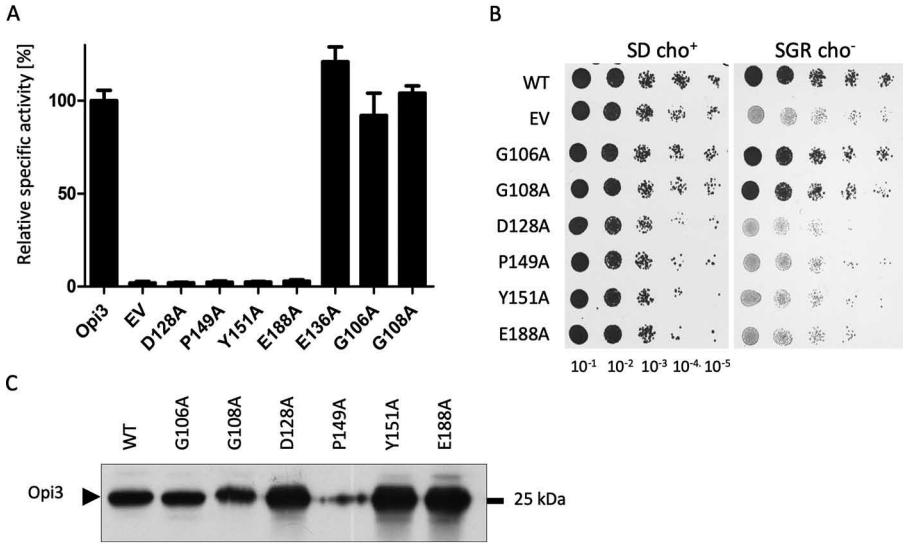

Figure 5. Mutations of proposed active site residues impair Opi3 activity. *A*, enzyme activity of Opi3 single amino acid mutants corresponding to residues potentially involved in the interaction with SAM. E136A is a random mutation used as control. Microsomes isolated from *cho2opi3* cells expressing the Opi3 mutants indicated were assayed for enzyme activity as detailed under "Experimental procedures." The specific activity of microsomes expressing WT Opi3-V5-His_6 construct was set at 100% (± S.D., $n = 3$); *EV* denotes empty vector control. *B*, complementation assay of Opi3 mutants with residues potentially involved in the binding of SAM replaced by alanine. A *cho2opi3* strain transformed with the pYES2.1 TOPO vector encoding WT or mutant Opi3 indicated was serially diluted on choline-free SGR to induce expression from the *GAL1* promoter and on SD medium supplemented with 1 mM choline (positive control) and incubated for 3 days at 30 °C. *C*, Western blotting comparing levels of expression of the Opi3 single amino acid mutants indicated to WT in samples corresponding to 20 μg of microsomal protein. Opi3 was detected using anti-V5 antibodies. The results are representative of two independent experiments.

ICMT and *T.c.* ICMT (27, 28) are conserved in Opi3 and PEMT, the P*X*Y (149–151 in Opi3) and EE (188–189 in Opi3) motifs in particular. The conservation of these motifs among ICMTs, ergosterol biosynthetic enzymes, and phospholipid methyltransferases was reported earlier (32).

Even though the quality of the model is not very high (QMEAN −4.62) (33), the overall predicted structure of C-terminal Opi3 resembles that of *M.a.* ICMT. Fig. 4*B* shows a superposition of the modeled C-terminal part of Opi3 (aa 98–206 of Opi3) on the structure of *M.a.* ICMT (aa 75–131) (27) and zooms in on the SAM-binding pocket, with the residues involved in SAH binding in ICMT and the corresponding conserved residues in Opi3 indicated. Positions of the P*X*Y and EE motifs in Opi3 match with those in *M.a.* ICMT, suggesting involvement in hydrogen bonding to SAM/SAH. Alanine substitutions of Pro-149, Tyr-151, Glu-188, and Asp-128, which may correspond to Glu-108 and Gln-189 that contact SAM in *M.a.* ICMT and *T.c.* ICMT, respectively (27, 28), abrogated Opi3 activity *in vitro* (Fig. 5*A*), and *in vivo* (Fig. 5*B*). Western blotting analysis showed that the impaired enzyme activity is not due to reduced expression levels of the Opi3 mutant proteins with the exception of the P149A mutant (Fig. 5*C*) that may be susceptible to proteolytic degradation. Interestingly, two conserved glycine residues (Gly-106 and Gly-108) in Opi3, which were implicated in SAM binding in PEMT (23), turned out not to influence the activity of Opi3 (Fig. 5, *A* and *B*), in agreement with their localization far from the putative SAM-binding site (Fig. 4).

Importantly, the model of the C-terminal part of Opi3 shows a re-entrant loop formed by TM IV, consistent with the topology of Opi3 proposed based on the SCAM analysis and predicted by PolyPhobius (Fig. 2*E*). However, in contrast to the PolyPhobius prediction, helix IV would start at Pro-149 rather than Val-138, and accordingly the re-entrant loop would be centered around Gly-166 rather than Gly-153 as in the PolyPhobius structure. We conclude that the active site of Opi3 is located at the cytosolic face of the ER membrane.

Discussion

The topology of integral membrane enzymes and the localization of their active sites is important for understanding their mechanism of action. For the occurrence of in *trans* catalysis, the localization of the enzyme's active site is of vital importance, because it determines the accessible lipid substrates. Here, Opi3, the phospholipid methyltransferase from yeast that has been proposed to convert lipid substrates in *trans* has been analyzed for membrane topology and localization of its active site.

Opi3 is a small (23 kDa) membrane protein insensitive to glycosylases like peptide:*N*-glycosidase and Endo H (Fig. 2*A* and data not shown) and therefore devoid of glycosylation. Topology prediction algorithms yielded four or five transmembrane domains varying in orientation and different localizations of the N terminus (Fig. 1). The discrepancies between topology predictions may be due to the ambiguous character of amino acid stretch 138–157 (Fig. 1 and Fig. S1*B*). Because of its low hydrophobicity (and high membrane insertion energy, $\Delta G_{app} = 7.87$ kcal/mol), most of the topology prediction algorithms we tested place it in the ER lumen. PolyPhobius is the exception that predicts this sequence to be in the membrane. Another potential reason for the discrepancies is the net negative charge of soluble domains B and C (Fig. S1*A*), resulting in a joint localization to the ER lumen and a predicted longer TM domain III forming a re-entrant loop (Fig. 1, *topologies 1–3*). Human PEMT shares 41% sequence identity with Opi3; therefore it is not surprising that its predicted topology is very similar (Fig. S1*A*).

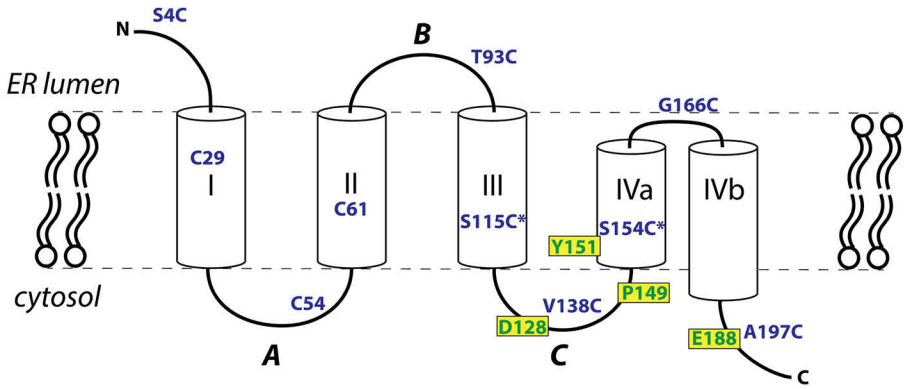

Figure 6. Proposed membrane topology of Opi3. The cartoon is based on SCAM analysis and the model of the structure of the C-terminal part of Opi3 (Fig. 4). The positions of the cysteines analyzed are indicated in *blue*. Those marked with *asterisks* do not complement the choline auxotrophy of a *cho2opi3* mutant (Fig. 2*B*). The proposed SAM-interacting amino acid residues are depicted in *yellow rectangles*. Alanine substitutions of Asp-128, Pro-149, Tyr-151, and Glu-188 inactivate Opi3; in case of Pro-149, we cannot exclude that inactivation is due to a decreased protein expression level (Fig. 5).

The data obtained by SCAM analysis of Opi3 and of functionally expressed human PEMT (Figs. 2*D* and 3*B*) combined with the modeling of the structure of the C-terminal half of Opi3 (Fig. 4*B*) yield a coherent picture of the arrangement of the TM helices in the membrane that is consistent with the topology predicted by PolyPhobius (Fig. 1*B*, *topology 6*) except for the position of the C-terminal helix–loop–helix. Both enzymes contain four TMs, of which the more extended TM IV forms an intramembranous turn or re-entrant loop and leaves the membrane with its C terminus at the cytosolic side. The existence of the re-entrant loop was experimentally proven by the Ubi–EMCS modification of V138C and A197C in Opi3 (Fig. 2*D*) and of A128C and S193C in PEMT (Fig. 3*B*), which flank TM IV. Compared with the PolyPhobius prediction (Fig. 1*B*), the model of the C-terminal structure (Fig. 4*B*) shifts TM IV ~10 amino acid residues closer to the C terminus (Fig. 4*A*), providing a much better fit with the hydrophobicity plot and the free energy for membrane insertion (Fig. 1*A*). Fig. 6 depicts the proposed topology of Opi3 based on the SCAM data (Fig. 2) and the structural model (Fig. 4).

The cytosolic localization of the C terminus of Opi3 was confirmed by DTR reporter analysis (Fig. 2*A*). The accessibility to Ubi–EMCS of native cysteine Cys-54 in Opi3 and of T39C in PEMT localized in soluble domain A, and the inability to derivatize N-terminal cysteines in both proteins demonstrates the N-out topology. Remarkably, Cys-54 in WT Opi3 is not accessible to Ubi–EMCS. This may be due to a nondeleterious alteration of the structure of cytosolic loop A caused by the triple cysteine mutation in the Cys-54 mutant, resulting in the exposure of cysteine 54 to the probe.

Previous analysis of the topology of human PEMT by bioinformatics and an endoproteinase protection assay suggested that the enzyme spans the ER membrane four times with both the N terminus and the C terminus facing the cytosol (13). Except for the cytosolic localization of the C terminus, the previously proposed topology is entirely opposite to the topology presented here. We speculate that the absence of proteolytic cleavage by Lys-C in cytosolic domains A and C observed previously (13) is due to steric hindrance by the proximity of the membrane or the protein's fold. In a later study, PEMT was shown to exist as two isoforms, of which the longer (26 kDa) contained an N-terminal glycosylated domain, indicating an ER luminal localization of the N terminus (34), consistent with the present data.

Opi3 and PEMT belong to the family of ICMT orthologues also including reductases involved in ergosterol synthesis that share sequence motifs involved in the binding of the soluble cofactors SAM and NADPH. The conserved motifs P*X*Y and EE were shown to be involved in binding SAH in the crystal structures of two ICMTs (27, 28, 32). In the predicted structure of Opi3's C-terminal part, these motifs attain virtually identical positions as in *M.a.* ICMT (Fig. 4*B*). Mutation of these residues abrogates Opi3 activity (Fig. 5), indicating that P*X*Y and EE are involved in SAM binding in Opi3. Importantly, additional residues in ICMT proteins located in the most C-terminal cytosolic loop contact SAM (Fig. 4*A*, *blue highlighted residues*). Mutation of Asp-128, the potential topological counterpart of Glu-108 that contacts SAM in *M.a.* ICMT (27), to alanine abrogated Opi3 activity, supporting the validity of the structural model.

Opi3 harbors a G*X*G motif at the same position of TM3 as human PEMT, which was shown to be required for PEMT activity and SAM binding by site-directed mutagenesis (23). Interestingly, mutation of the G*X*G motif in Opi3 did not affect Opi3 activity. According to our Opi3/PEMT topology model, the G*X*G motif resides within the membrane quite distant from the P*X*Y/EE motifs, suggesting that the deleterious effects of mutating G*X*G in PEMT may be indirect.

In the proposed model of Opi3 topology, the SAM-binding residues are located at the membrane-cytosol interface (Figs. 4*B* and 6), as expected based on the membrane peripheral localization of the methyl-accepting headgroups of PMME and PDME. The conservation of the C-terminal part corresponding to TM domain IV, soluble domain C, and the C-terminal stretch including the SAM-binding residues between different organisms (Bacteria, Archaea, yeast, insects, and mammals) and different enzymes (reductases and methyltransferase) indicates that this is a universal fold/motif involved in binding of adenosyl-containing cofactors to integral membrane enzymes converting membrane resident substrates (sterol, prenylated protein, and phospholipid) (31–33). The localization of Opi3's active site is consistent with the proposed mechanism of in

Table 1
Strains and plasmids used in this study

	Genotype or description	Source
Strain		
cho2opi3	*MATα his3Δ1 leu2Δ0 lys2Δ0 ura3Δ0 cho2::KanMX opi3::LEU2*	Ref. 49
STY50	*MAT***a** *his4-401 leu2-3, −112 trp1-1 ura3-52 hol1-1 suc2::LEU2* A	Ref. 50
Plasmid		
pYES2.1 TOPO	2μ, *GAL1* promoter, *URA3*, C-terminal V5- His_6 tag	Invitrogen
pYES2.1 TOPO-*OPI3*	WT *OPI3* and derived mutant alleles in pYES2.1 TOPO	This study
pYES2.1 TOPO-*PEMT*	WT *PEMT* and derived mutant alleles in pYES2.1 TOPO	This study
pJK90-*OST4*	2μ, *URA3*, *OST4-HA-SUC2-HIS4C* under control of the *TPI* promoter	Ref. 50
pJK90-EV	pJK90-*OST4* lacking *OST4-HA-SUC2-HIS4C construct*	This study
pJK90-*OPI3*	*OPI3-HA-SUC2-HIS4C* under control of the *TPI* promoter	This study

trans catalysis, as well as with conventional catalysis in *cis*. Further insight into the catalytic mechanism awaits elucidation of a high-resolution structure containing bound lipid substrate.

Experimental procedures

Strains, media, and culture conditions

Yeast strains and plasmids used are listed in Table 1. Yeast strains were cultured in YPD medium (1% yeast extract, 2% peptone, and 2% glucose) or glucose-based synthetic defined (SD) medium under aerobic conditions at 30 °C (35). For expression of Opi3 and PEMT under the *GAL1* promoter from the pYES2.1 TOPO vector, 2% galactose and 1% raffinose were used as carbon sources in SGR medium lacking uracil. Growth of Opi3 and PEMT single cysteine mutants was tested by serial dilution on synthetic defined medium plates containing 75 μM inositol, lacking or supplemented with 1 mM choline (36), after preculture to mid-log phase in glucose-based SD medium containing choline and inositol.

Bioinformatics

Protein sequence alignments were performed using the UniProt ALIGN server (37) or EMBOSS needle (51) as indicated. Hydrophobicity plot was generated by ExPASy ProtScale (38) using the Kyte and Doolittle scale (39), and topology predictions were generated using TOPCONS (40). ΔG values for membrane insertion were calculated using DGPRED (41). The 3D structure of the Opi3 C terminus was predicted using the HHpred platform (42) and SWISS-MODEL (43).

Molecular biology

The sequences of all primers used in this study are listed in Table S1. All PCRs were performed using Phusion polymerase (Thermo Fisher). PCR products were purified using Wizard® SV gel and PCR clean-up system (Promega). Plasmids were isolated from *Escherichia coli* using QIAprep spin miniprep kit (Qiagen).

The *OPI3* gene was PCR-amplified using genomic DNA from BY4742 and primers A-for and A-rev and cloned into the pGEM-T easy vector (Promega) according to the manufacturer's instructions. For expression in yeast, the Opi3 ORF was PCR-amplified from the pGEM-T-OPI3 plasmid using primers B-for and B-rev, and the intron-free PEMT ORF from plasmid hPEMT-pCI (13), kindly provided by Dr. D. Vance, was amplified using primers C-for and C-rev. Both PCR products were ligated into the pYES2.1 TOPO vector (Invitrogen) in frame with the C-terminal V5-His_6 tag according to the manufacturer's instructions generating pYES2.1 TOPO-*OPI3* and pYES2.1 TOPO-*PEMT*. Single amino acid substitutions in Opi3-V5-His_6 and PEMT-V5-His_6 were introduced by PCR-mediated site-directed mutagenesis using the QuikChange kit (Agilent Technologies) and the primers listed in Table S1. Plasmids were multiplied in *E. coli* DH5a cells and transformed into the *cho2opi3* strain (44).

DTR was added to the C terminus of Opi3 by homologous recombination of an insert containing the *OPI3* gene with the linearized plasmid pJK90-*OST4* carrying the *OST4-HA-SUC2-HIS4C* construct (a kind gift of Dr. A. Conzelmann (45)). The insert was generated using genomic DNA and the primers D-for and D-rev. Plasmid pJK90-*OST4* was linearized with SmaI, and transformed with the insert in a 1:10 molar ratio into STY50 cells. The generated plasmid pJK90-*OPI3* carried the construct *OPI3-HA-SUC2-HIS4C* under the constitutive triosephosphate isomerase promoter. Transformants were selected on −ura plates. The pJK90-EV plasmid lacking *OST4-HA-SUC2-HIS4C* was prepared by reverse PCR of pJK90-*OST4* plasmid and primers E-for and E-rev. PCR product was phosphorylated using T4 polynucleotide kinase (NEB), digested with DpnI (NEB), and circularized using T4 DNA ligase (NEB).

Preparation of microsomes

cho2opi3 cells expressing Opi3 or PEMT constructs were grown to log phase (A_{600} 1.0) in SGR medium. The cells were harvested by centrifugation for 10 min at 3600 × *g*, washed in 1 mM EDTA (pH 7.4), and subjected to subcellular fractionation (46). Briefly, the cells were incubated at 30 °C for 10 min at 2 ml/g of wet cells in 0.1 M Tris-HCl, pH 7.4, 10 mM DTT, spun down at 3600 × *g* for 5 min, and washed in buffer S (1.2 M sorbitol, 50 mM Tris-HCl, pH 7.4). The cells were resuspended at 3 ml/g of wet cells in buffer S supplemented with 0.5 mg of Zymolyase (Amsbio, 100 kU/mg) per g of cells and incubated at 30 °C for 30 min. Spheroplasts were diluted with ice-cold buffer S and collected by centrifugation at 3600 × *g* for 5 min at 4 °C. Pelleted spheroplasts were resuspended in ice cold 0.6 M sorbitol, 10 mM Tris-HCl, pH 7.4, containing protease inhibitors (cOmplete protease inhibitor mixture, Roche; 1 tablet/50 ml), and homogenized by 10 strokes with a Dounce homogenizer on ice. Unbroken cells and nuclei were removed by centrifugation at 3600 × *g* for 5 min at 4 °C.

The cell homogenate (supernatant) was centrifuged at 12,000 × *g* for 15 min to remove mitochondria. The microsomal fraction was isolated by ultracentrifugation of the supernatant at 100,000 × *g* for 1 h at 4 °C. The pellet was resuspended in buffer A (50 mM Tris-HCl, pH 7.5, 0.6 M sorbitol), flash-

frozen as aliquots in liquid nitrogen, and stored at −80 °C. Aliquots were thawed only once. Microsomal protein concentration was determined using the BCA assay (Pierce) in the presence of 0.1% SDS and using BSA as a standard.

Determination of protein topology

Synthesis of ubiquitin—EMCS and cysteine scanning—Ubi–EMCS was prepared according to Pagac *et al.* (24). Briefly, 2.3 mM ubiquitin (Sigma) and 3.35 mM sulfo–EMCS (6-maleimidocaproic acid sulfo-*n*-succinimidyl ester; Thermo Fisher Scientific) dissolved in 50 mM sodium phosphate, pH 7.4, were mixed in a ratio 3:2 (v/v), respectively, in a total volume of 500 μl and incubated for 40 min at room temperature on a rotary wheel. The product was washed and concentrated in the same buffer using a Centricon centrifugal filter unit (3000 molecular weight cutoff). Sorbitol was added to 0.6 M, yielding a final concentration of Ubi–EMCS of 4.5 mM (assuming 100% reaction yield), and aliquots were snap-frozen and stored at −20 °C. For cysteine scanning, microsomes (15 μg of microsomal protein) were mixed with 45 nmol of Ubi–EMCS in 0.1 M sodium phosphate, pH 7.4, 0.6 M sorbitol, 5 mM $MgCl_2$ with or without 1% SDS in a total reaction volume of 50 μl and incubated for 1 h on ice. For each series of reactions, a freshly thawed aliquot of Ubi–EMCS was used. The reaction was quenched by adding 5 μl of 1 M DTT and incubating for 5 min at room temperature. Next, SDS-PAGE loading buffer was added, and samples were incubated at 56 °C for 10 min. Proteins (15 μg) were separated on 15% SDS–polyacrylamide gels and analyzed by Western blotting using anti-V5 monoclonal antibodies (Thermo Scientific), or anti-Kar2p.

Dual topology reporter analysis—STY50 yeast cells transformed with pJK90-EV or pJK90-*OPI3* encoding Opi3-DTR were serially diluted on SD −ura and SD −ura −his plates containing 6 mM histidinol and incubated for 4 days at 30 °C. To examine glycosylation of the DTR constructs, heavy microsomes were isolated from cells cultured on SD −ura medium. Microsomes corresponding to 10 μg of total membrane protein were prepared according to the manufacturer's instructions prior to incubation with 1000 units of Endo H (NEB) for 2 h at 37 °C with gentle agitation. The samples were separated on an 8% SDS–polyacrylamide gel and visualized on Western blotting using anti-HA antibodies (Abcam).

Measurement of methyltransferase activity

Enzyme activity of Opi3 and PEMT was assayed as the amount (nmol) of [^{3}H]methyl group from *S*-adenosyl-L-[*methyl*-^{3}H]methionine ([^{3}H]SAM) incorporated into chloroform soluble material per min per mg protein (14, 18). Large unilamellar vesicles (LUVs) consisting of 1,2-dioleoyl-*sn*-glycero-3-phosphoethanolamine-*N*-methyl (PMME; Avanti Polar Lipids) served as lipid substrate and were prepared by hydrating a lipid film in buffer A followed by 10 freeze-thaw cycles (in dry ice/ethanol and a water bath at 30 °C) and 20× extrusion through a 200-nm pore-size Whatman nucleopore track-etched polycarbonate (hydrophilic) membrane (GE Healthcare) using the Avanti mini-extruder set. A 100-μl reaction mixture containing microsomes (0.05 mg protein/ml), LUV (0.4 mM PMME), and 1 mM SAM (Sigma) containing 5000 dpm [^{3}H]-SAM/nmol (10 Ci/mmol; PerkinElmer Life Sciences) in buffer A was incubated at 30 °C in a shaking thermomixer (650 rpm) for 10 min. The reaction was stopped by adding 375 μl of $CHCl_3$:methanol:0.1 M HCl, 10:5:1 (v/v/v), followed by lipid extraction (47). The incorporated [^{3}H]methyl was quantitated by liquid scintillation counting. The phospholipid concentrations of the PMME stock solution in chloroform, and the LUV preparations were determined according to Rouser *et al.* (48).

Author contributions—G. P., M. A. K., and A. I. P. M. d. K. conceptualization; G. P. data curation; G. P., M. A. K., and A. I. P. M. d. K. formal analysis; G. P. validation; G. P., M. F. R., and M. A. K. investigation; G. P. visualization; G. P., M. F. R., and M. A. K. methodology; G. P. writing-original draft; G. P., M. F. R., M. A. K., and A. I. P. M. d. K. writing-review and editing; A. I. P. M. d. K. supervision; A. I. P. M. d. K. project administration.

Acknowledgments—We thank Dr. Xue Bao for help with the experiments, Sander Filon and Ruud Cox for technical support, Dr. Andreas Conzelmann and Dr. Dennis Vance for sharing plasmids and strains, and Dr. Ineke Braakman for the anti-Kar2p antibody.

References

1. Kodaki, T., and Yamashita, S. (1987) Yeast phosphatidylethanolamine methylation pathway: cloning and characterization of two distinct methyltransferase genes. *J. Biol. Chem.* **262,** 15428–15435 Medline
2. McGraw, P., and Henry, S. (1989) Mutations in the *Saccharomyces cerevisiae* OPI3 gene: effects on phospholipid methylation, growth and cross-pathway regulation of inositol synthesis. *Genetics* **122,** 317–330 Medline
3. Summers, E. F., Letts, V. A., McGraw, P., and Henry, S. A. (1988) *Saccharomyces cerevisiae* cho2 mutants are deficient in phospholipid methylation and cross-pathway regulation of inositol synthesis. *Genetics* **120,** 909–922 Medline
4. Kanipes, M. I., and Henry, S. A. (1997) The phospholipid methyltransferases in yeast. *Biochim. Biophys. Acta* **1348,** 134–141 CrossRef Medline
5. Ridgway, N. D., and Vance, D. E. (1988) Kinetic mechanism of phosphatidylethanolamine N-methyltransferase. *J. Biol. Chem.* **263,** 16864–16871 Medline
6. Vance, D. E. (2013) Physiological roles of phosphatidylethanolamine *N*-methyltransferase. *Biochim. Biophys. Acta* **1831,** 626–632 CrossRef Medline
7. Keogh, M. R., Courtney, P. D., Kinney, A. J., and Dewey, R. E. (2009) Functional characterization of phospholipid *N*-methyltransferases from *Arabidopsis* and soybean. *J. Biol. Chem.* **284,** 15439–15447 CrossRef Medline
8. Fagone, P., and Jackowski, S. (2013) Phosphatidylcholine and the CDP-choline cycle. *Biochim. Biophys. Acta* **1831,** 523–532 CrossRef Medline
9. Hölzl, G., and Dörmann, P. (2019) Chloroplast lipids and their biosynthesis. *Annu. Rev. Plant Biol.* **70,** 51–81 CrossRef Medline
10. Sadhu, M. J., Moresco, J. J., Zimmer, A. D., Yates, J. R., 3rd, and Rine, J. (2014) Multiple inputs control sulfur-containing amino-acid synthesis in *Saccharomyces cerevisiae*. *Mol. Biol. Cell* **25,** 1653–1665 CrossRef Medline
11. Ye, C., Sutter, B. M., Wang, Y., Kuang, Z., and Tu, B. P. (2017) A metabolic function for phospholipid and histone methylation. *Mol. Cell* **66,** 180–193.e8 CrossRef Medline
12. Danne, L., Aktas, M., Gleichenhagen, J., Grund, N., Wagner, D., Schwalbe, H., Hoffknecht, B., Metzler-Nolte, N., and Narberhaus, F. (2015) Membrane-binding mechanism of a bacterial phospholipid *N*-methyltransferase. *Mol. Microbiol.* **95,** 313–331 CrossRef Medline
13. Shields, D. J., Lehner, R., Agellon, L. B., and Vance, D. E. (2003) Membrane topography of human phosphatidylethanolamine *N*-methyltransferase. *J. Biol. Chem.* **278,** 2956–2962 CrossRef Medline
14. Gaynor, P. M., and Carman, G. M. (1990) Phosphatidylethanolamine methyltransferase and phospholipid methyltransferase activities from

Saccharomyces cerevisiae: Enzymological and kinetic properties. *Biochim. Biophys. Acta* **1045,** 156–163 CrossRef Medline
15. Holthuis, J. C., and Menon, A. K. (2014) Lipid landscapes and pipelines in membrane homeostasis. *Nature* **510,** 48–57 CrossRef Medline
16. Hoffmann, P. C., and Kukulski, W. (2017) Perspective on architecture and assembly of membrane contact sites. *Biol. Cell* **109,** 400–408 CrossRef Medline
17. Prinz, W. A. (2014) Bridging the gap: Membrane contact sites in signaling, metabolism, and organelle dynamics. *J. Cell Biol.* **205,** 759–769 CrossRef Medline
18. Janssen, M. J. F. W., de Jong, H. M., de Kruijff, B., and de Kroon, A. I. P. M. (2002) Cooperative activity of phospholipid-*N*-methyltransferases localized in different membranes. *FEBS Lett.* **513,** 197–202 CrossRef Medline
19. Quon, E., Sere, Y. Y., Chauhan, N., Johansen, J., Sullivan, D. P., Dittman, J. S., Rice, W. J., Chan, R. B., Di Paolo, G., Beh, C. T., and Menon, A. K. (2018) Endoplasmic reticulum–plasma membrane contact sites integrate sterol and phospholipid regulation. *PLoS Biol.* **16,** e2003864 CrossRef Medline
20. Tavassoli, S., Chao, J. T., Young, B. P., Cox, R. C., Prinz, W. A., de Kroon, A. I., and Loewen, C. J. R. (2013) Plasma membrane: endoplasmic reticulum contact sites regulate phosphatidylcholine synthesis. *EMBO Rep.* **14,** 434–440 CrossRef Medline
21. Henrich, E., Löhr, F., Pawlik, G., Peetz, O., Dötsch, V., Morgner, N., de Kroon, A. I., and Bernhard, F. (2018) Lipid conversion by cell-free synthesized phospholipid methyltransferase Opi3 in defined nanodisc membranes supports an in *trans* mechanism. *Biochemistry* **57,** 5780–5784 CrossRef Medline
22. Brooks, C. L., Morrison, M., and Lemieux, M. J. (2013) Rapid expression screening of eukaryotic membrane proteins in *Pichia pastoris*. *Protein Sci.* **22,** 425–433 CrossRef Medline
23. Shields, D. J., Altarejos, J. Y., Wang, X., Agellon, L. B., and Vance, D. E. (2003) Molecular dissection of the *S*-adenosylmethionine-binding site of phosphatidylethanolamine *N*-methyltransferase. *J. Biol. Chem.* **278,** 35826–35836 CrossRef Medline
24. Pagac, M., de la Mora, H. V., Duperrex, C., Roubaty, C., Vionnet, C., and Conzelmann, A. (2011) Topology of 1-acyl-*sn*-glycerol-3-phosphate acyltransferases SLC1 and ALE1 and related membrane-bound *O*-acyltransferases (MBOATs) of *Saccharomyces cerevisiae*. *J. Biol. Chem.* **286,** 36438–36447 CrossRef Medline
25. Pagac, M., Vazquez, H. M., Bochud, A., Roubaty, C., Knöpfli, C., Vionnet, C., and Conzelmann, A. (2012) Topology of the microsomal glycerol-3-phosphate acyltransferase Gpt2p/Gat1p of *Saccharomyces cerevisiae*. *Mol. Microbiol.* **86,** 1156–1166 CrossRef Medline
26. Liu, Q., Siloto, R. M., Snyder, C. L., and Weselake, R. J. (2011) Functional and topological analysis of yeast acyl-CoA:diacylglycerol acyltransferase 2, an endoplasmic reticulum enzyme essential for triacylglycerol biosynthesis. *J. Biol. Chem.* **286,** 13115–13126 CrossRef Medline
27. Yang, J., Kulkarni, K., Manolaridis, I., Zhang, Z., Dodd, R. B., Mas-Droux, C., and Barford, D. (2011) Mechanism of isoprenylcysteine carboxyl methylation from the crystal structure of the integral membrane methyltransferase ICMT. *Mol. Cell* **44,** 997–1004 CrossRef Medline
28. Diver, M. M., Pedi, L., Koide, A., Koide, S., and Long, S. B. (2018) Atomic structure of the eukaryotic intramembrane RAS methyltransferase ICMT. *Nature* **553,** 526–529 CrossRef Medline
29. Kim, H., Melén, K., and von Heijne, G. (2003) Topology models for 37 *Saccharomyces cerevisiae* membrane proteins based on C-terminal reporter fusions and predictions. *J. Biol. Chem.* **278,** 10208–10213 CrossRef Medline
30. McWilliam, H., Li, W., Uludag, M., Squizzato, S., Park, Y. M., Buso, N., Cowley, A. P., and Lopez, R. (2013) Analysis tool web services from the EMBL-EBI. *Nucleic Acids Res.* **41,** W597–W600 CrossRef Medline
31. Li, X., Roberti, R., and Blobel, G. (2015) Structure of an integral membrane sterol reductase from *Methylomicrobium alcaliphilum*. *Nature* **517,** 104–107 CrossRef Medline
32. Romano, J. D., and Michaelis, S. (2001) Topological and mutational analysis of *Saccharomyces cerevisiae* Ste14p, founding member of the isoprenylcysteine carboxyl methyltransferase family. *Mol. Biol. Cell* **12,** 1957–1971 CrossRef Medline
33. Benkert, P., Biasini, M., and Schwede, T. (2011) Toward the estimation of the absolute quality of individual protein structure models. *Bioinformatics* **27,** 343–350 CrossRef Medline
34. Morita, S. Y., Takeuchi, A., and Kitagawa, S. (2010) Functional analysis of two isoforms of phosphatidylethanolamine *N*-methyltransferase. *Biochem. J.* **432,** 387–398 CrossRef Medline
35. De Smet, C. H., Vittone, E., Scherer, M., Houweling, M., Liebisch, G., Brouwers, J. F., de Kroon, A. I. (2012) The yeast acyltransferase Sct1p regulates fatty acid desaturation by competing with the desaturase Ole1p. *Mol. Biol. Cell* **23,** 1146–1156 CrossRef Medline
36. Griac, P., Swede, M. J., and Henry, S. A. (1996) The role of phosphatidylcholine biosynthesis in the regulation of the INO1 gene of yeast. *J. Biol. Chem.* **271,** 25692–25698 CrossRef Medline
37. Pundir, S., Martin, M. J., and O'Donovan, C.; UniProt Consortium (2016) UniProt Tools. *Curr. Prot. Bioinformatics* **53,** 1.29.1–1.29.15 CrossRef Medline
38. Gasteiger, E., Gattiker, A., Hoogland, C., Ivanyi, I., Appel, R. D., and Bairoch, A. (2003) ExPASy: the proteomics server for in-depth protein knowledge and analysis. *Nucleic Acids Res.* **31,** 3784–3788 CrossRef Medline
39. Kyte, J., and Doolittle, R. F. (1982) A simple method for displaying the hydropathic character of a protein. *J. Mol. Biol.* **157,** 105–132 CrossRef Medline
40. Bernsel, A., Viklund, H., Hennerdal, A., and Elofsson, A. (2009) TOPCONS: consensus prediction of membrane protein topology. *Nucleic Acids Res.* **37,** W465–W468 CrossRef Medline
41. Hessa, T., Meindl-Beinker, N. M., Bernsel, A., Kim, H., Sato, Y., Lerch-Bader, M., Nilsson, I., White, S. H., and von Heijne, G. (2007) Molecular code for transmembrane-helix recognition by the Sec61 translocon. *Nature* **450,** 1026–1030 CrossRef Medline
42. Söding, J., Biegert, A., and Lupas, A. N. (2005) The HHpred interactive server for protein homology detection and structure prediction. *Nucleic Acids Res.* **33,** W244–W248 CrossRef Medline
43. Biasini, M., Bienert, S., Waterhouse, A., Arnold, K., Studer, G., Schmidt, T., Kiefer, F., GalloCassarino, T., Bertoni, M., Bordoli, L., and Schwede, T. (2014) SWISS-MODEL: modelling protein tertiary and quaternary structure using evolutionary information. *Nucleic Acids Res.* **42,** W252–W258 CrossRef Medline
44. Gietz, R. D. (2014) Yeast transformation by the LiAc/SS carrier DNA/PEG method. In *Yeast Genetics: Methods and Protocols* (Smith, J. S., and Burke, D. J., eds) pp. 1–12, Springer, New York
45. Kim, H., Yan, Q., Von Heijne, G., Caputo, G. A., and Lennarz, W. J. (2003) Determination of the membrane topology of Ost4p and its subunit interactions in the oligosaccharyltransferase complex in *Saccharomyces cerevisiae*. *Proc. Natl. Acad. Sci. U.S.A.* **100,** 7460–7464 CrossRef Medline
46. Daum, G., Böhni, P. C., and Schatz, G. (1982) Import of proteins into mitochondria. Cytochrome b2 and cytochrome c peroxidase are located in the intermembrane space of yeast mitochondria. *J. Biol. Chem.* **257,** 13028–13033 Medline
47. Bligh, E. G., and Dyer, W. J. (1959) A rapid method of total lipid extraction and purification. *Can. J. Biochem. Physiol.* **37,** 911–917 CrossRef Medline
48. Rouser, G., Fleischer, S., and Yamamoto, A. (1970) Two dimensional thin layer chromatographic separation of polar lipids and determination of phospholipids by phosphorus analysis of spots. *Lipids* **5,** 494–496 CrossRef Medline
49. Boumann, H. A., Chin, P. T., Heck, A. J., De Kruijff, B., and De Kroon, A. I. (2004) The yeast phospholipid N-methyltransferases catalyzing the synthesis of phosphatidylcholine preferentially convert di-C16:1 substrates both in vivo and in vitro. *J. Biol. Chem.* **279,** 40314–40319 CrossRef Medline
50. Strahl-Bolsinger, S., and Scheinost, A. (1999) Transmembrane topology of Pmt1p, a member of an evolutionarily conserved family of protein *O*-mannosyltransferases. *J. Biol. Chem.* **274,** 9068–9075 CrossRef Medline
51. Li, W., Cowley, A., Uludag, M., Gur, T., McWilliam, H., Squizzato, S., Park, Y. M., Buso, N., and Lopez, R. (2015) The EMBL-EBI bioinformatics web and programmatic tools framework. *Nucleic Acids Res.* **43,** W580–W584 CrossRef Medline